**Showcasing research from Institute for New Energy Materials & Low-Carbon Technologies, Tianjin University of Technology & Qualification of Products Supervision & Inspection Institute of Technology, Xinjiang.**

Single-unit-cell-thick layered electrocatalysts: from synthesis to application

Single-unit-cell-thick layered electrocatalysts possess distinctive properties against bulk counterparts owing to their superior specific surface areas and massive active sites. This minireview not only focuses on their thermal and liquid exfoliation synthesis approaches but also summarizes their performances for water splitting, carbon dioxide reduction and rechargeable zinc-air batteries.
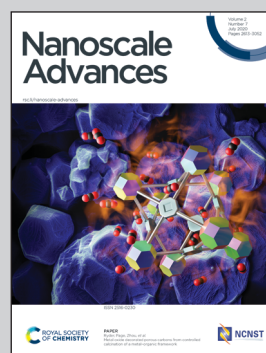
ROYAL SOCIETY
OF **CHEMISTRY**

rsc.li/nanoscale-advances

MINIREVIEW

Check for updates

Single-unit-cell-thick layered electrocatalysts: from synthesis to application

Sanshuang Gao,[a] Yifan Liu, [ID][b] Hongyi Li,*[c] Xijun Liu [ID][a] and Jun Luo [ID]*[a]

Electrocatalysts are critical for water splitting, carbon dioxide reduction, and zinc–air battery. However, the low-exposed surface areas of bulk electrocatalysts usually limit the complete utilization of active sites. Ultrathin electrocatalysts have noteworthy advantages in maximizing the use of active sites. Among the pioneering works on such performing catalysts, the development of single-unit-cell-thick layered electrocatalysts (STLEs) has attracted extensive attention owing to their superior specific surface area and large number of vacancies, which can provide abundant available surface active sites. Therefore, this minireview provides recent advances in STLE synthesis and applications, which are helpful for electrocatalysis-oriented researchers. Finally, the future perspectives and challenges for developing high-performance STLEs are proposed.

1. Introduction

During the last decade, the aggravation of energy crisis and global warming was witnessed. Therefore, developing eco-friendly strategies to produce clean and renewable energy sources is accelerated.[1–3] Among various innovative options, photo- and electrocatalytic technologies have been regarded as efficient strategies for developing appropriate alternative energy sources to replace fossil fuels.[4,5] Of them, the materials used for

electrochemical water splitting, carbon dioxide reduction reaction (CO_2RR), and rechargeable zinc–air batteries (ZABs) exhibit excellent catalytic activity, stability, selectivity, and faradaic efficiency (FE), allowing these reactions to be employed as promoters of clean-renewable energy sources.[6–8] For instance, water splitting contains two half-reactions, *i.e.*, hydrogen evolution reaction (HER), occurring on the cathode, and oxygen evolution reaction (OER), taking place on the anode.[9] Hydrogen fuel, obtained by HER, has an extremely high mass-based energy density and environmental-friendly characteristics.[10–12] OER is essential not only for water splitting but also for the charging process occurring in ZABs, one of the next-generation energy storage batteries.[13,14] Low-carbon number hydrocarbons obtained by CO_2RR are feedstocks and renewable fuels with a high potential in solving both energy crisis and global warming.[15] The core of these processes is the electrocatalyst, which should have a large number of highly dispersed active

[a]Center for Electron Microscopy and Tianjin Key Lab of Advanced Functional Porous Materials, Institute for New Energy Materials & Low-Carbon Technologies, School of Materials Science and Engineering, Tianjin University of Technology, Tianjin 300384, China. E-mail: jluo@tjut.edu.cn

[b]College of Physics and Optoelectronic Engineering, Shenzhen University, Shenzhen 518060, China

[c]Qualification of Products Supervision & Inspection Institute of Technology, Xinjiang Uygurs Autonomous Region, Urumqi 830011, China. E-mail: 422340661@qq.com

Sanshuang Gao received his M.S. degree from College of Materials Science and Engineering, Anhui University of Science and Technology, China, in 2018. His research interests mainly focus on the design, synthesis and applications of nanomaterials.

Yifan Liu received his PhD degree from Heidelberg University, Germany, in 2019. His current scientific interests focus on nanomaterials, optics, and light–matter interaction.

sites.[16] However, the agglomeration is a common phenomenon encountered in the development of such catalysts. Hence, a part of the active sites do not participate in the reactions, and thus the catalyst does not work at full capacity.[17,18] Therefore, exploring appropriate methods for the synthesis of electrocatalysts without aggregates is significant to properly address the energy and environmental crisis.[19]

Ultrathin nanomaterials (UNMs), benefiting from their unique properties such as thin thickness, large specific surface area, abundant active sites, excellent electroconductibility, and preferential diffusion paths, were developed in the attempts to overcome the agglomeration issues and to provide materials abundant of accessible active sites.[20] For instance, Liu et al. prepared an ultrathin chiffon-like structure to overcome the agglomeration of layered double hydroxides, and Geenen et al. developed ultrathin $NiSi_2$ films to avoid morphological agglomeration.[21,22] Thus, UNMs are widely applied in electrocatalysis, photocatalysis, biosensors, biomedicine, energy storage, and energy conversion.[23–25] For example, Zhang et al.

prepared ultrathin Co_3O_4 and $Co(OH)_2$ nanosheet arrays, and Dinh et al. reported ultrathin porous NiFeV for efficient electrocatalytic water splitting.[26,27] Li et al. proposed ultrathin CeO_2 nanoflakes loaded on graphene for ZABs, and Esrafilzadeh et al. reported atomically thin CeO_2 for CO_2RR.[28,29]

Although extensive works on UNM for electrocatalysis have been done, the preparations methods and potential applications still need to be upgraded.[30] Many reviews mainly focusing on the synthesis (e.g., top-down and bottom-up approaches, including liquid exfoliation, thermal exfoliation, chemical vapor deposition, and wet-chemical synthesis[31–34]) and applications (e.g., photocatalysts,[35] electrocatalysts,[36–38] biomedicine, and biosensing[39,40]) of ultrathin layered nanomaterials have been published.[31–41] Nevertheless, there are quite few reviews discussing the single-unit-cell-thick layered electrocatalysts (STLEs, thickness normally less than 1.0 nm), which essentially approaches the fundamental limit thickness of UNMs.[42] That is, the STLE thickness is the fundamental lower limit of the UNM thickness,[42] and the name of UNMs is used to represent single-/few-/multiple-unit-cell-thick nanomaterials in general.[43] It should also be noted that the thickness of unit-cell-thick sheet (UCS) is equivalent to the STLE thickness.[44,45] Generally, monolayer means single layer, which is also single-unit-cell-thick but from the view of layered structures.[46–48] The concept of single-unit-cell-thick is from the view of crystal structures and more general.[44] Unlike conventional UNMs, STLEs provide a thinner monolayer for exposing more surface-active sites and a larger number of structural defects, which changes the intrinsic activity. Specifically, single-unit-cell-thick layered double hydroxides (LDHs) with defect-rich surface-active sites exhibited excellent electric conductivity and spin-polarization characteristics, which were improved by the single-unit-cell thickness, in OER.[49] Co_3O_4-based STLEs with distinct oxygen vacancies on the surface were prepared to understand the relationship between vacancies and catalytic activity in CO_2RR.[50] Single-unit-cell-thick $CoSe_2$ in which 66.7% Co^{2+} acted as surface-active sites were prepared for OER performance.[51] Therefore, all these outcomes highlight the significance of the morphostructural properties, particularly the thickness and

Hongyi Li received the B.S. and PhD degrees in Mechanics, Physics and Chemistry Materials from Beijing Institute of Technology, Beijing, in 2008 and Xinjiang Physics and Chemistry Institute of Technology, Chinese Academy of Science, in 2013, respectively. From 2011 to 2012, he was a Joint PhD candidate in Northwestern University, Chicago, the U.S. From 2013 to 2014, he was a Senior Engineer, and since 2015 he has been a professor with the institute of Products Quality Supervision and Inspection, Urumqi, Xinjiang Uruguay Autonomous Region, China. His research interest includes Materials Science, Solid State of Chemistry and Chemistry Industry of Technology.

Xijun Liu received his PhD degree from College of Science, Beijing University of Chemical Technology in 2014. His current scientific interests focus on nanomaterials, heterogeneous catalysis, and materials design for catalysts and energy conversion/storage.

Jun Luo received his B.S. (2001) and PhD (2006) from Tsinghua University, China. Then, he worked as a postdoc in Warwick University and a research fellow in Oxford University, UK. In 2011, he joined Tsinghua University as an associate professor. In 2015, he moved to Tianjin University of Technology and is a full professor in Center for Electron Microscopy. His research interests focus on low-dimensional materials and their electron microscopy and optical imaging.

vacancies of STLEs for catalytic performance. However, the preparation of such solids is challenging and several strategies were proposed.

In this minireview, we thoroughly summarize the latest progress in the synthesis of STLEs for electrocatalytic water splitting, CO_2RR, and ZABs. Synthetic strategies (*i.e.*, thermal and liquid exfoliation techniques) are in-depth discussed. The characterization results are also discussed. Subsequently, the electrocatalytic performance (*i.e.*, catalytic activity, durability, selectivity, and FE) of STLEs is described aiming to highlight the recent advances in electrocatalysis. Therefore, this minireview aims to provide ideas for the design and synthesis of STLEs and discuss the challenges and perspectives for future applications.

2. Synthesis of STLEs

The structural properties, *e.g.*, vacancies and thickness, have been considered as major factors affecting the quantity of active sites and electric conductivity of STLEs.[23,52] Usually, electrocatalysts display a low number of active sites on the surfaces with low coordination numbers due to the stronger electrostatic interactions between layers which is detrimental for the catalytic activity. Therefore, pioneering works have devoted efforts to overcoming the electrostatic interactions between layers aiming to control the structural defects and the electronic properties of STLEs.[53] In the following, the published synthetic strategies, *i.e.*, thermal and liquid exfoliation, are detailed.

2.1 Thermal exfoliation synthesis

Solvothermal/hydrothermal exfoliation techniques are widely used in preparing single-unit-cell-thick layered photocatalysts. Normally, the synthesis is performed in a stainless steel autoclave, at high temperature and autogeneous pressure.[54–57] For instance, Huang *et al.* synthesized single-unit-cell-thick Bi_2WO_6 monolayers with surface tungsten vacancies by hydrothermal method;[58] Di *et al.* employed solvothermal method to synthesize ultrathin BiOBr nanosheets, which was further used as template to obtain single-unit-cell-thick Bi_2WO_6.[59] However, there is still little literature, focusing on the solvothermal/ hydrothermal fabrication of STLEs, correlate to electrocatalytic applications. Thus, this section has cited three representative thermally exfoliation strategies, which successfully synthesize STLEs *via* solvothermal/hydrothermal intermediates.

As illustrated in Fig. 1a. Gao *et al.* transferred cetyltrimethyl ammonium bromide (CTAB) and $Co(acac)_3$ into a Teflon-lined autoclave with a mixture of ethylene glycol and distilled water (reacting under 180 °C for 20 h). Then, the self-assembled intermediates were thermally exfoliated (320 °C for 5 min) under air and O_2 gaseous environment, respectively.[50] The as-obtained thickness of V_O-rich and V_O-poor Co_3O_4 correspond to 0.84 nm (Fig. 1b and c), which fairly agrees with Co_3O_4 single-unit-cell. Similarly, as shown in Fig. 1d and e. Liang *et al.* blended Co^{2+} and Se into a mixture of diethylenetriamine and distilled water, maintained at 180 °C for 30 h. Subsequently, the assembled intermediates were thermally exfoliated (350 °C for 1 h) under atmosphere conditions for generating single-unit-cell-thick $CoSe_2$, which presents 0.66 nm height.[51] Besides, our group has dissolved Zn^{2+}, Co^{2+}, NH_4F, and urea into distilled water, both of the mixed solution and rinsed Ti substrate were then transferred into Teflon-lined autoclave, which was maintained at 100 °C for 10 h. Subsequently, the hydrothermal growth of Zn-doped α-$Co(OH)_2$ was placed in 1 M NaOH and 1 M $NaBH_4$ solution at 5 °C for 2 h, and calcined at 250 °C for 3 h under an Ar atmosphere (Fig. 1f).[44] In the light of discussing results, it can be stated that
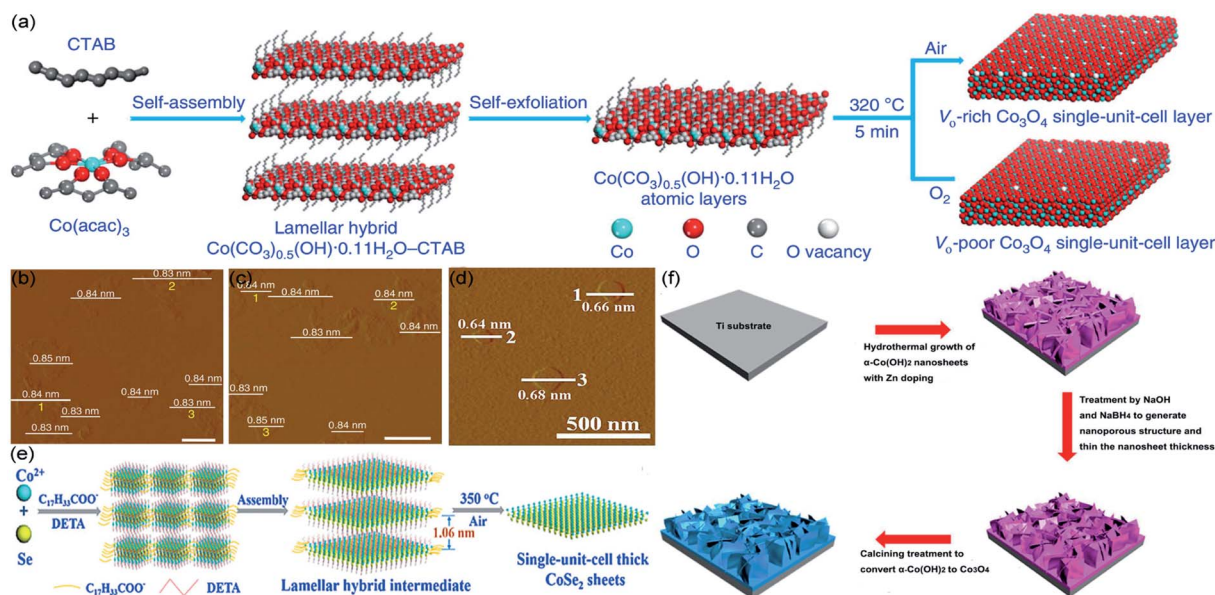

Fig. 1 For thermal exfoliation. (a) Scheme for preparing single–unit–cell–thick layered Co_3O_4; AFM images of (b) V_O–rich and (c) V_O–poor single–unit–cell–thick layered Co_3O_4, respectively. Reproduced from ref. 50. Copyright 2017, Springer Nature. (d) AFM image and (e) scheme for fabricating single–unit–cell–thick layered $CoSe_2$, respectively. Reproduced from ref. 51. Copyright 2015, Wiley-VCH. (f) Scheme for generating Zn-doped Co_3O_4 single-unit-cell. Reproduced from ref. 44. Copyright 2018, Elsevier.

thermal methods have a great potential to prepare efficient STLEs for electrocatalytic reactions.

It is shown that these strategies of synthesis are very convenient to obtain STLEs due to the facile tuning of structural defects and morphology of STLEs by changing the temperature and gaseous environment during thermal treatment. Whereas, the automatic reaction leads to difficultly analyze the mechanistic principles of thermal process. Furthermore, thermal exfoliation requires complicated multi-step procedures (*i.e.*, solvothermal/hydrothermal process and calcined treatment), which possibly cause potential safety risks, especially for the high-temperature solvothermal process.

2.2 Liquid exfoliation synthesis

Liquid exfoliation is a simple method to prepare monolayers by which the van der Waals interactions between layers is controlled. Typically, the multilayer solid precursor is immersed into a liquid, and ultrasounds are applied to overcome the attractive forces between layers and separate them. For instance, Miao *et al.* adopted a liquid exfoliation strategy to synthesize misfit-layered-structured $Bi_2Sr_2Co_2O_{8+\delta}$ (BSCO) nanosheets, which possess a single-unit-cell-thick structure (Fig. 2a and b).[5] The bulk BSCO (misfit-layered CoO_2 and SrO–BiO–BiO–SrO) involves weak van der Waals forces between BiO layers, which can be overcome to exfoliate the BSCO structure and obtain stable independent monolayers. Basically, the BSCO crystals were immersed in *N*-methyl-2-pyrrolidone and an ultrasonic treatment was applied in ice water for 24 h to obtain single-unit-cell-thick BSCO nanosheets. As seen in Fig. 2b, displaying atomic force microscopy (AFM) image and corresponding height results, the one-unit-cell BSCO has an average thickness of 3 nm, corresponding to the thickness of BSCO single unit cell.[60] Moreover, Yang *et al.* proposed a self-surface charge exfoliation utilizing ultrasound treatment to fabricate single-unit-cell-thick $ZnIn_2S_4$ from multilayered $ZnIn_2S_4$.[61] As illustrated in Fig. 2c, $InCl_3$ and $Zn(OOCCH_3)_2$ were transferred into distilled water with refluxing and then sonicated continuously for 30 min to obtain the single-unit-cell-thick $ZnIn_2S_4$.

During the synthetic process, a high amount of S^{2-} was adsorbed onto the surface of bulk $ZnIn_2S_4$, causing a strong negative charge on the surface. As a result, the interactions between layers were weakened and the Coulombic repulsion promoted their separation.[62] Each layer has a thickness of $\sim$2.5 nm, corresponding to the thickness of a unit cell in the (001) direction of $ZnIn_2S_4$ (Fig. 2d).

Liquid exfoliation can be achieved by different strategies, such as shear force, ultrasonication, or thermal energy, to exfoliate multilayered crystals and avoid other heteroatoms polluting catalyst.[63,64] However, there are still some shortcomings, restricting the commercial applications of liquid exfoliation methods, such as continuous noise during ultrasonication and strongly ultrasonic energy destroying fragile layers.

3. Application of STLEs

With a graphene-like geometric structure, STLEs expose far more surface-active sites and low-coordinated surfaces compared to bulk catalysts, which endow them with plentiful dangling bonds for enhancing catalytic performance. Furthermore, benefitting from their unique morphostructural properties and strong synergistic effect with substrates, STLEs are expected to exhibit improved electric conductivity and spin-polarization characteristics as effective electrocatalysts in electrochemical energy storage and conversion. Therefore, the pioneering electrochemical applications, *i.e.*, water splitting (including HER and OER), CO_2RR, and ZABs, are favored and highlighted in the following discussions.

3.1 STLEs for HER

The hydrogen, due to its zero-carbon emission, is regarded as a clean and renewable energy source to replace fossil fuels.[65] In the last decade, platinum-based catalysts have been considered as state-of-the-art catalysts for industrial hydrogen production.[66] Nevertheless, the high cost impedes their large-scale applications.[67] Therefore, developing low-cost catalysts to replace platinum-based ones has become a hot topic in HER-

Fig. 2 Schematic illustration of ultrasonic exfoliation of bulk (a) BSCO and (c) $ZnIn_2S_4$; AFM images of single–unit–cell (b) BSCO and (d) $ZnIn_2S_4$. (a and b) Reproduced from ref. 5. Copyright 2018, American Chemical Society. (c and d) Reproduced from ref. 61. Copyright 2017, Springer Nature.

oriented research. Recently, high-purity hydrogen was obtained by water splitting over transition metal dichalcogenides as HER catalysts.[68] The monolayer molybdenum disulfide (M-MoS$_2$, which is also single-unit-cell-thick MoS$_2$) catalysts, benefiting from the high density of edges hosting the active sites, have been used in HER with high improved catalytic efficiency.[69,70]

For instance, Su et al. have employed ultrathin alumina mask-assisted nanopore patterning to synthesize high-density porous MoS$_2$ (HDP-MoS$_2$).[47] This unit-cell-thick HDP-MoS$_2$ is richer in edges, as compared with the pristine monolayer MoS$_2$ (M-MoS$_2$). As Fig. 3a illustrated, large-area M-MoS$_2$ (before ion beam etching) displays a triangular flake-like morphology with a thickness of ~0.7 nm. Revealing M-MoS$_2$ maintains structural integrity during the transfer process. Then, the ion beam etching was applied to generate high-density nanopores with an average diameter of 50 nm in uncovered MoS$_2$. It should be noted that the transfer of HDP-MoS$_2$ from the SiO$_2$ substrate used for its preparation to the glassy carbon electrode (GCE) for HER was accomplished by spincoating polystyrene, HF etch, water cleaning and floating, and polystyrene pyrolysis. This process enhanced the adhesion between HDP-MoS$_2$ and GCE, leading to a stable HER current density within 10 000 s. Further, the pores in a monolayer structure increase the edge atom ratio, which promotes a high HER potential of −385 mV for HDP-MoS vs. reversible hydrogen electrode (RHE) at 10 mA cm^{-2} (Fig. 3c). Due to the excellent performance obtained for HER, the controllable edge engineering method can be extended to other materials.

Wang et al. utilized the interlayer spaces of Mg–Al LDH to grow the two-dimensional (2D) M-MoS$_2$, which suspended in water with the large-scale monolayer ratio (approximate 95%).[71] As shown in Fig. 3b, the thickness and lateral size of M-MoS$_2$ are ~1 and 89 nm, respectively, based on the measurement of 400 unit-cell-thick particles. Overpotential and durability are critical indicators used to assess the performance of a catalyst for HER. The as-obtained HER activity of M-MoS$_2$ exhibited a lower onset overpotential of 85 mV and an overpotential of 210 mv (vs. RHE) at 10 mA cm^{-2}, which are significantly lower than bulk MoS$_2$ (see Fig. 3d). This should be because compared with bulk MoS$_2$, M-MoS$_2$ owns larger ratios of edge atoms, which can expose massive active sites and facilitate electronic conduction. These are beneficial for catalyzing HER and thereby can lead to a better HER performance. The polarization curves, showing stability without any obvious change, were obtained before and after 1000 cyclic voltammetry cycles. All these results reveal that M-MoS$_2$ has indeed a real potential to increase the efficiency of HER process.

3.2 STLEs for OER

The theoretical electrode potential of O$_2$ generation is 1.23 V (vs. RHE), which indicates that considerable potentials (above theoretical potential) have to be applied on the electrode to promote OER.[72] However, a high overpotential is energy-consuming, which makes the OER process unsustainable. At present, a hot research topic is the optimization of electro-catalysts to enhance the performance in OER. Fortunately, single-unit-cell-thick electrocatalysts proved to be appropriate materials to solve this challenge. The synthesized electro-catalysts could decrease the overpotential and thus make an economically feasible OER.

Gao et al. employed the co-precipitation method to synthesize 2D single-unit-cell-thick LDH nanosheets (including CoNi-, NiFe-, CoFe-, and ZnCo-LDH NSs).[46] According to the AFM image, the LDH nanosheets with hexagonal-like morphology, lateral sizes of ~40 nm, and an average thickness of ~1.3 nm are monodispersed (Fig. 4a and b). The thickness value between single- and two-layer LDH NSs (synthesized through liquid exfoliation method) probably be enhanced by the residual anions and/or solvents. Density functional theory (DFT) calculations reveal that CoFe- and NiFe-LDHs accelerate electronic
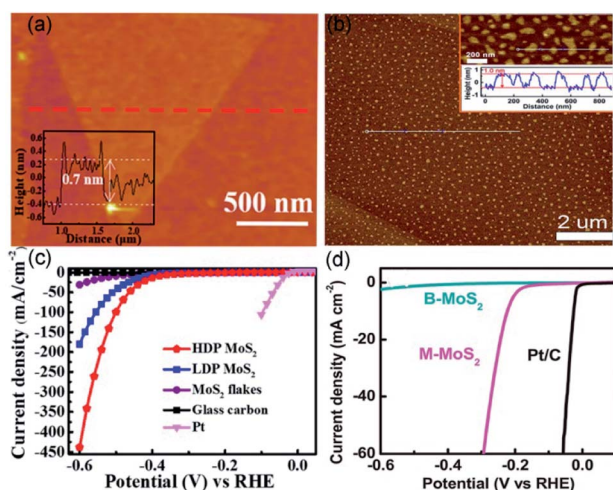

Fig. 3 AFM images and the corresponding heights of (a) HDP-MoS$_2$ precursor and (b) M-MoS$_2$. The polarization curves of (c) HDP-MoS$_2$ and (d) M-MoS$_2$ in comparison with other catalysts. (a and c) Reproduced from ref. 47. Copyright 2018, American Chemical Society. (b and d) Reproduced from ref. 71. Copyright 2019, Elsevier.
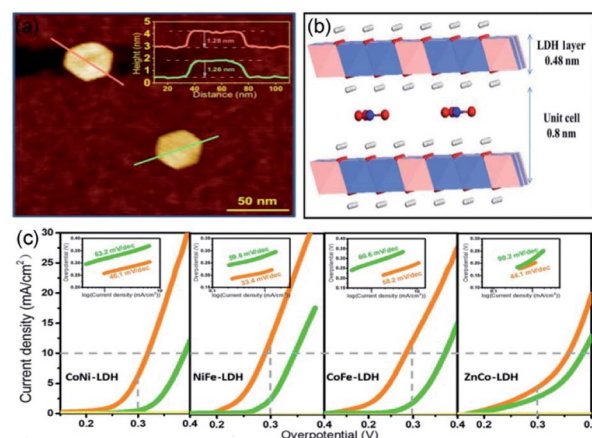

Fig. 4 (a) AFM image and the corresponding heights of individual LDH. (b) Schematic illustration of the interlayer spacing of single-unit-cell-thick LDH NS. (c) Polarization curves and Tafel plots of bimetallic LDH NS (orange line) and bulk LDH (green line). Reproduced from ref. 46. Copyright 2018, Springer Nature.

spin-polarization, reduce energy gaps, and hence enhance electron mobility.[46] Furthermore, the single-unit-cell-thick thickness exhibits vast surface defects, which can serve as catalytically active sites. To investigate OER performance, polarization curves were tested, in which the loading technique of the bulk and LDH NSs catalysts was dropping and evaporating the homogeneous catalyst inks onto fresh GCE. As shown in Fig. 4c, as compared with bulk LDH (green line), bimetallic LDH NSs (orange line) exhibit superior overpotential and Tafel slopes. Among these bimetallic LDH NSs, CoFe-LDH NSs revealed the lowest overpotential (280 mV at 10 mA cm^{-2}) and excellent TOF values (5.5 mF cm^{-2} at 300 mV overpotential), whereas NiFe-LDHs NSs showed the highest electrocatalytic activity (Tafel slope of 33.4 mV per decade and FE of nearly 100%). Moreover, compared with the commercial IrO$_2$ catalysts, the NiFe-LDH NSs was active for 8 h, suggesting a high stability.

Our group has applied a synthesis strategy, combining hydrothermal treatment, etching, and calcination, to synthesize nanoporous Zn-doped Co$_3$O$_4$ sheets with single-unit-cell thickness and lateral surfaces (NPCoO-UCSs, in which UCS denotes unit-cell-thick sheet) for efficient OER.[44] Morphological characterization in Fig. 5a reveals that partial interconnecting NPCoO-UCSs stand on the Ti foil, which generated considerable lateral surfaces and many nanopores, and the HR-TEM image shows 0.2 nm interplanar spacing, which belongs to (004) plane of Co$_3$O$_4$.[73] As seen in Fig. 5b, AFM image measurement shows that the heights of NPCoO-UCSs (0.84 ± 0.03 nm) are very close to that of single-unit-cell-thick (0.81 nm).[74] The NPCoO arrays growing on Ti foils were directly used as electrochemical electrodes with a mass loading of 0.45 mg cm^{-2}. To compare the OER performance of different UCS heights, the etching durations (0, 1.0, 1.5, 2.5, and 3 h) were controlled to obtain distinctive polarization curves and TOF values of NPCoO. Different from those control samples (CoO-0 h, NPCoO-1 h, NPCoO-1.5 h, NPCoO-2.5 h, and CoO-3 h), NPCoO-UCSs (prepared by 2 h etching) possessed more nanopores and oxygen vacancies, both of which can accelerate the transfer of intermediates and electrons, resulting in higher catalytic performance.[75] In Fig. 5c and d the onset potential and over-potential (calculating from 10 mA cm^{-2}) of NPCoO-UCSs in 0.1 M KOH are 1.369 and 0.172 V, respectively. Furthermore, the high activity of NPCoO-UCSs maintains 50 000 s for OER and 500 h for overall water splitting without obviously attenuating.

3.3 STLEs for CO$_2$RR

The high emissions of CO$_2$ have impacted the climate, causing global warming and threatening sustainable development.[76] CO$_2$ electrochemical reduction into reusable low-carbon energy sources is an efficient route for sustainable recycling of carbon resources.[77] Thus, recent investigations focused on developing suitable ultrathin electrocatalysts for CO$_2$RR.[78,79]

Our group has illustrated that Li-intercalation/exfoliation method allowed to obtain a monolayered SnS$_2$ (M-SnS$_2$) catalyst with excellent catalytic activity in CO$_2$RR.[48] As illustrated in Fig. 6a, AFM image and three different areas of corresponding heights showed an average thickness of 0.58 ± 0.04 nm, which is closing to that of the single-unit-cell thickness of SnS$_2$, i.e., 0.59 nm (Fig. 6c). The FE of formate product specific to SnS$_2$ monolayers is ~100% at −0.8 V vs. RHE (Fig. 6b). In addition, the long-term durability of the STLE was proved by the 80 h of activity without an obvious decrease. We also studied the probable chemical pathways involved in the conversion of CO$_2$ by DFT calculations. Fig. 6d–f, reveal that HCOO*, COOH*, and H* are the main competitive intermediates of the reactions
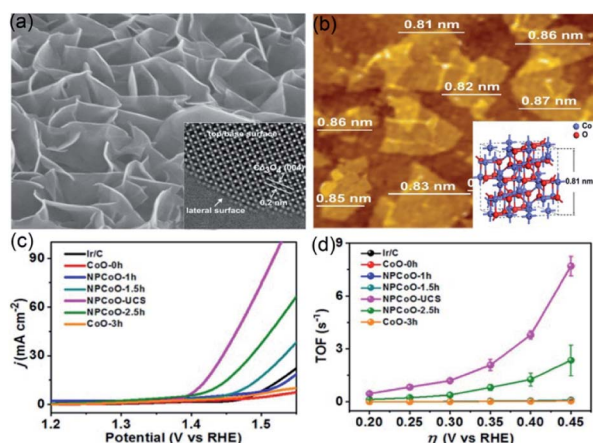

Fig. 5 (a) Low-magnification and high-resolution TEM images of NPCoO-UCSs. (b) Top-view AFM image of NPCoO-UCSs, the measurable thickness close to the inserting 3D model of standard Co$_3$O$_4$ unit cell. (c) OER polarization curves of NPCoO-UCSs and other catalysts. (d) TOF vs. thickness curves of NPCoO-UCSs and other catalysts. Reproduced from ref. 44. Copyright 2018, Elsevier.
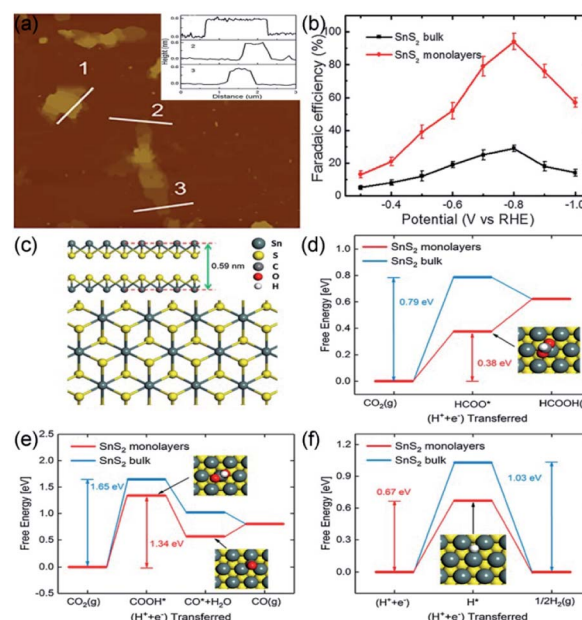

Fig. 6 (a) AFM image and the corresponding heights and (b) FEs of formate over SnS$_2$ monolayer at various applied potentials. (c) Atomic side and top models of single-unit-cell SnS$_2$. (d and e) Free energy results of CO$_2$ reduction to (d) HCOOH and (e) CO by SnS$_2$ monolayer and bulk surface. (f) Free energy results of HER by SnS$_2$ monolayer and bulk surface. Reproduced from ref. 48. Copyright 2018, Elsevier.

leading to HCOOH, CO, and H_2, respectively. Notably, it was found that the lowest Gibbs free energy (0.38 eV) belongs to HCOO* intermediate, which is formed on the (001) surface of M-SnS_2. By contrary, the Gibbs free energy of HCOO* formation on bulk SnS_2 was higher (0.79 eV). This phenomenon was mainly caused by the higher electron density of M-SnS_2. Therefore, our group proposed a promising route to prepare an efficient and robust STLE for CO_2 reduction.

3.4 STLEs for ZABs

Due to their high theoretical energy density (1084 W h kg^{-1}), excellent safety, and low cost, ZABs are considered as one of the next-generation batteries to replace lithium-ion batteries.[80,81] Oxygen evolution reaction (OER, which is the charge process) and oxygen reduction reaction (ORR, which is the discharge process) are the half-reactions occurring at the working electrode in ZABs.[13] The overpotential of OER and half-wave/onset potential of ORR significantly affect the charge–discharge processes of ZABs. Yet, the use of commercial noble-metal-based materials, such as Pt/C, RuO_2, and IrO_2, as catalysts, restricts the large-scale development of ZABs. Developing cost-effective, high-performance, and robust catalysts to replace precious-metal-based catalysts is challenging, but it will be the key to the widespread application of ZABs. Recently, the transition metal oxides and hydroxides loaded on reduced graphene oxide (rGO) were successfully applied as STLEs for OER/ORR processes of ZABs due to the advantages of STLE structure already discussed.[82,83] In these composite materials, the rGO acts as a current collector to accelerate the transfer of electrons.

Wang et al. have proposed Br$^-$-intercalation, NO_3^--exchange, and exfoliation methods to gradually expand the interlayer distance of bulk CoNi-LDH for obtaining CoNi-NS monolayers.[82] The delaminated CoNi-NSs were then flocculated and calcined together with GO to obtain CoNi-NS/rGO composites. As seen in Fig. 7a, the AFM image shows an average thickness of CoNi-NS monolayers of 0.7–0.8 nm, corresponding to the 0.8 nm of the

CoNi-LDH monolayer. The single-unit-cell-thick structure of CoNi-NS monolayers and electrical conductivity of rGO endow the CoNi-NS/rGO composite with outstanding electrocatalytic activity and durability in ORR and OER under alkaline conditions. A homogeneous CoNi-NS/rGO ink, hybrid with Ketjenblack carbon, was dropped onto GCE with a loading of 0.48 mg cm^{-2}. For OER charge process, an overpotential of 330 mV (vs. RHE) was obtained at 10 mA cm^{-2}, for ORR discharge progress, the half-wave potential was of 0.85 V (vs. RHE), and the H_2O_2 yield was less than 7% (Fig. 7b and c). Benefitting from the effective properties of the bifunctional material, CoNi-NS/rGO exhibited stable rechargeability (more than 350 cycles) and a 300 mW cm^{-2} power density with a durable polarization gap (0.8 V at 10 mA cm^{-2}) (Fig. 7d). Therefore, the authors proposed an efficient strategy to synthesize single-unit-cell-thick CoNi-NS/ rGO composites for ZAB, especially since the delamination and flocculation methods are suitable for fabricating other types of STLEs. In addition, the substrate effect should also be considered for explaining the changes of intrinsic activity. As reported by Wang et al.,[82] the rGO substrate, acting as a current collector, accelerates the electron transfer during the charge–discharge process of zinc-air batteries with CoNi-NS/rGO. Uosaki et al. find that the interaction between monolayer h-BN and the Au substrate facilitates the binding and activation of O_2 molecules, and thereby significantly reduces the overpotential of oxygen reduction reaction.[83]

Li et al. reported a facile and continuous method to synthesize layered Co_3O_4/nitrogen-doped rGO (Co_3O_4/N-rGO) composite, which can be assembled and knitted into flexible and wearable ZAB. In addition, the wearable device was made of low-cost materials, i.e., zinc wire, chiffon band, and carbon fibers.[84] As shown in Fig. 8a, AFM image reveals that the thickness of Co_3O_4 nanosheets is 0.8 nm, corresponding to the single-unit-cell-thick of Co_3O_4 (0.81 nm). Noteworthy, compared with Pt/C and RuO_2, Co_3O_4/N-rGO exhibited better ORR and
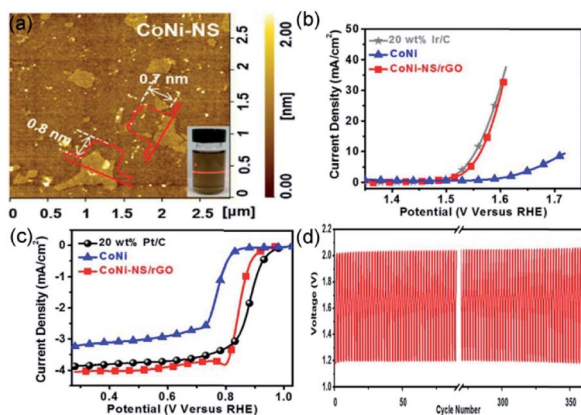

Fig. 7 (a) AFM image of CoNi-NS and photograph of CoNi-NS suspension. Polarization curves of CoNi-NS/rGO, CoNi, and commercial catalysts for (b) OER and (c) ORR. (d) Charge and discharge cycling curves of CoNi-NS/rGO at 10 mA cm^{-2}. Reproduced from ref. 82. Copyright 2019, Elsevier.
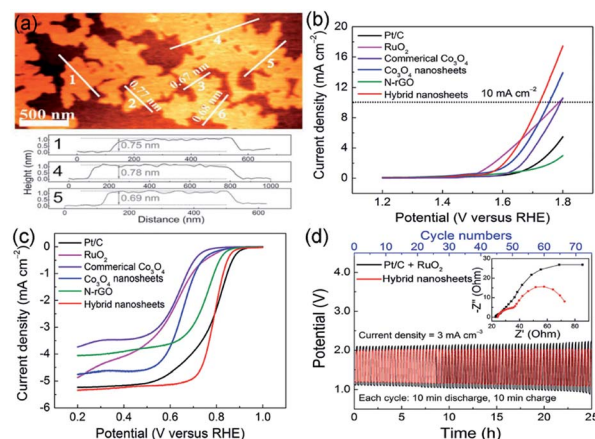

Fig. 8 (a) AFM image and the corresponding height profiles of Co_3O_4 NS. (b and c) Linear sweep voltammetry curves of Co_3O_4/N-rGO, Co_3O_4-NS, N-rGO, commerical Co_3O_4, RuO_2, and Pt/C. (d) Charge and discharge cycling curves of Co_3O_4/N-rGO and electrochemical impedance spectroscopy (EIS) spectrum of ZAB. Reproduced from ref. 84. Copyright 2018, Wiley-VCH.

OER performances, *i.e.*, lower half-wave potential $E_{1/2}$ (0.79 V *vs.* RHE) for ORR and overpotential $E_{j=10}$ (490 mV *vs.* RHE) for OER (Fig. 8b and c). Moreover, the charge–discharge potentials of ZAB appropriate for polarization curves, indicating better rechargeability of the novel composite material. Additionally, because the layered structure enlarged the surface-to-surface contact between Co_3O_4/N-rGO and the electrode, the cycling stability of ZAB showed a better rechargeability without obvious potential gap increase than the Pt/C + RuO_2 catalyst. As a result, the charge–discharge potentials of the two catalysts approximated 2.0 V (Co_3O_4/N-rGO) and 1.2 V (Pt/C + RuO_2) within 75 cycles for 25 h, respectively (Fig. 8d). The outcomes of that article are promising for ZAB applications in wearable electronics.

4. Conclusions and perspectives

STLEs (layer thickness generally less than 1.0 nm) are excellent candidates for commercial applications based on electrolytic processes. This minireview summarizes the latest strategies applied for the synthesis of STLEs and their applications in various fields. For STLE synthesis, both liquid exfoliation and thermal treatments under autogeneous pressure are considered as efficient strategies to fabricate high-performance STLEs. Liquid exfoliation approach is a facile way, allowing to overcome the weak forces between adjacent layers to separate them into individual layers; the thermal exfoliation approach depends on the optimized reaction parameters to produce STLEs efficiently. The catalytic activity of STLEs is maximized by the high surface area and vacancies, which increase the amount of active sites.

However, despite the progress made in the synthesis of STLEs, their widespread application is still narrow. In this minireview, we attempt to identify those limitations and succinctly present them, as follows. (1) To obtain STLEs, liquid exfoliation and thermal processes are associated with noise and safety risks, respectively. More importantly, some reaction mechanisms and conditions take insufficient account of preparing monolayered electrocatalysts, such as the multi-step thermally exfoliation methods requiring time-consuming (typically, more than 10 h) solvothermal/hydrothermal procedure and high-temperature (typically, more than 250 °C) calcination, which are uneconomic for large-scale achieving STLEs. Besides, liquid exfoliation methods are unsuitable for exfoliating multi-layer electrocatalysts in which the structural integrity of the assembly is maintained by strong interactions. Therefore, alternative strategies, such as chemical vapor deposition and epitaxial growth, should be adopted to go further into the preparation of a wide range of STLEs. (2) Regarding the application, although remarkable pioneering works have devoted efforts to STLEs, the challenges are related to the stability of STLEs, which remains controversial, due to that the single-unit-cell-thick structure will more easily transform into other characteristics during the whole reaction process. In addition, the performance of STLEs highly depends on the monolayer thickness and number of vacancies, and thus a degree of uncertainty over the relationship between performance and structure still

exists. Thus, more advanced characterization techniques and DFT calculations are needed to shed more light on this relationship. Yet, despite all these challenges, STLEs have proven to have excellent electrochemical properties due to the suppressed agglomeration of particles and large amounts of active sites exposed, which encourage the researches in the area.

Conflicts of interest

There are no conflicts to declare.

Acknowledgements

Notes and references

1 W. Ma, X. Liu, C. Li, H. Yin, W. Xi, R. Liu, G. He, X. Zhao, J. Luo and Y. Ding, *Adv. Mater.*, 2018, **30**, 1801152.

2 S. Shen, X. Peng, L. Song, Y. Qiu, C. Li, L. Zhuo, J. He, J. Ren, X. Liu and J. Luo, *Small*, 2019, **15**, 1902229.

3 F. Lü, H. Bao, Y. Mi, Y. Liu, J. Sun, X. Peng, Y. Qiu, L. Zhuo, X. Liu and J. Luo, *Sustainable Energy Fuels*, 2020, **4**, 1012–1028.

4 M. Jiang, J. Li, J. Li, Y. Zhao, L. Pan, Q. Cao, D. Wang and Y. Du, *Nanoscale*, 2019, **11**, 9654–9660.

5 X. Miao, S. Zhou, L. Wu, J. Zhao and L. Shi, *ACS Sustainable Chem. Eng.*, 2018, **6**, 12337–12342.

6 C. Guan, W. Xiao, H. Wu, X. Liu, W. Zang, H. Zhang, J. Ding, Y. P. Feng, S. J. Pennycook and J. Wang, *Nano Energy*, 2018, **48**, 73–80.

7 R. Wang, F. Kapteijn and J. Gascon, *Chem.–Asian J.*, 2019, **14**, 3452–3461.

8 M. Li, F. Luo, Q. Zhang, Z. Yang and Z. Xu, *J. Catal.*, 2020, **381**, 395–401.

9 L. Fu, F. Yang, G. Cheng and W. Luo, *Nanoscale*, 2018, **10**, 1892–1897.

10 S. Geng, W. Yang and Y. S. Yu, *J. Catal.*, 2019, **375**, 441–447.

11 X. Wang, Y. Zheng, W. Sheng, Z. J. Xu, M. Jaroniec and S.-Z. Qiao, *Mater. Today*, 2020, DOI: 10.1016/j.mattod.2019.12.003.

12 H. Liu, X. Peng and X. Liu, *ChemElectroChem*, 2018, **5**, 2963–2974.

13 S. Li, C. Cheng, X. Zhao, J. Schmidt and A. Thomas, *Angew. Chem., Int. Ed.*, 2018, **57**, 1856–1862.

14 S. Clark, A. R. Mainar, E. Iruin, L. C. Colmenares, J. A. Blázquez, J. R. Tolchard, Z. Jusys and B. Horstmann, *Adv. Energy Mater.*, 2020, **10**, 1903470.

15 P. De Luna, R. Quintero-Bermudez, C.-T. Dinh, M. B. Ross, O. S. Bushuyev, P. Todorović, T. Regier, S. O. Kelley, P. Yang and E. H. Sargent, *Nat. Catal.*, 2018, **1**, 103–110.

16 X. Liu, H. Yang, J. He, H. Liu, L. Song, L. Li and J. Luo, *Small*, 2018, **14**, 1704049.

17 S. Dou, L. Tao, R. Wang, S. El Hankari, R. Chen and S. Wang, *Adv. Mater.*, 2018, **30**, 1705850.

18 P. M. Shafi, N. Joseph, A. Thirumurugan and A. C. Bose, *Chem. Eng. J.*, 2018, **338**, 147–156.

19 S. Shrestha, B. Wang and P. Dutta, *Adv. Colloid Interface Sci.*, 2020, **279**, 102162.

20 H. Chem Soc RevZhang, M. Chhowalla and Z. Liu, *Chem. Soc. Rev.*, 2018, **47**, 3015–3017.

21 J. Liu, X. Bai, Q. Liu, R. Chen, X. Jing, B. Li, R. Li and J. Wang, *J. Electrochem. Soc.*, 2018, **165**, A784–A792.

22 F. A. Geenen, K. van Stiphout, A. Nanakoudis, S. Bals, A. Vantomme, J. Jordan-Sweet, C. Lavoie and C. Detavernier, *J. Appl. Phys.*, 2018, **123**, 075303.

23 Y. Li, J. Yin, L. An, M. Lu, K. Sun, Y. Q. Zhao, F. Cheng and P. Xi, *Nanoscale*, 2018, **10**, 6581–6588.

24 Z. Liu, S. Zhang, H. Lin, M. Zhao, H. Yao, L. Zhang, W. Peng and Y. Chen, *Biomaterials*, 2018, **155**, 54–63.

25 B. Li, C. Lai, L. Qin, C. Chu, M. Zhang, S. Liu, X. Liu, H. Yi, J. He, L. Li, M. Li and L. Chen, *Adv. Colloid Interface Sci.*, 2020, **560**, 701–713.

26 L. Zhang, B. Liu, N. Zhang and M. Ma, *Nano Res.*, 2017, **11**, 323–333.

27 K. N. Dinh, P. Zheng, Z. Dai, Y. Zhang, R. Dangol, Y. Zheng, B. Li, Y. Zong and Q. Yan, *Small*, 2018, **14**, 1703257.

28 D. Esrafilzadeh, A. Zavabeti, R. Jalili, P. Atkin, J. Choi, B. J. Carey, R. Brkljača, A. P. O'Mullane, M. D. Dickey, D. L. Officer, D. R. MacFarlane, T. Daeneke and K. Kalantar-Zadeh, *Nat. Commun.*, 2019, **10**, 865.

29 X. Li, Z. Liu, L. Song, D. Wang and Z. Zhang, *Electrochim. Acta*, 2018, **263**, 561–569.

30 T. I. Kim, I. J. Park and S. Y. Choi, *Nano Lett.*, 2020, **20**, 3740–3746.

31 M. Luo, Y. Yang, Y. Sun, Y. Qin, C. Li, Y. Li, M. Li, S. Zhang, D. Su and S. Guo, *Mater. Today*, 2019, **23**, 45–56.

32 K. ZHAO, W. Zhu, S. Liu, X. Wei and Z. He, *Nanoscale Adv.*, 2020, **2**, 536–562.

33 H. Zhang, *ACS Nano*, 2015, **9**, 9451–9469.

34 C. Tan, X. Cao, X. J. Wu, Q. He, J. Yang, X. Zhang, J. Chen, W. Zhao, S. Han, G. H. Nam, M. Sindoro and H. Zhang, *Chem. Rev.*, 2017, **117**, 6225–6331.

35 J. Xiong, P. Song, J. Di and H. Li, *Appl. Catal., B*, 2019, **256**, 117788.

36 J. Lai and S. Guo, *Small*, 2017, **13**, 1702156.

37 W. Zhang and K. Zhou, *Small*, 2017, **13**, 1700806.

38 J. Di, C. Yan, A. D. Handoko, Z. W. Seh, H. Li and Z. Liu, *Mater. Today*, 2018, **21**, 749–770.

39 X. Ge, Z. Xia and S. Guo, *Adv. Funct. Mater.*, 2019, **29**, 1900318.

40 K. V. Sreekanth, S. Sreejith, S. Han, A. Mishra, X. Chen, H. Sun, C. T. Lim and R. Singh, *Nat. Commun.*, 2018, **9**, 369.

41 J. Xu, X. Chen, Y. Xu, Y. Du and C. Yan, *Adv. Mater.*, 2019, **32**, 1806461.

42 D. Li, S. Hao, G. Xing, Y. Li, X. Li, L. Fan and S. Yang, *J. Am. Chem. Soc.*, 2019, **141**, 3480–3488.

43 M. Golalikhani, Q. Lei, R. U. Chandrasena, L. Kasaei, H. Park, J. Bai, P. Orgiani, J. Ciston, G. E. Sterbinsky, D. A. Arena, P. Shafer, E. Arenholz, B. A. Davidson, A. J. Millis, A. X. Gray and X. X. Xi, *Nat. Commun.*, 2018, **9**, 2206.

44 X. Liu, W. Xi, C. Li, X. Li, J. Shi, Y. Shen, J. He, L. Zhang, L. Xie, X. Sun, P. Wang, J. Luo, L.-M. Liu and Y. Ding, *Nano Energy*, 2018, **44**, 371–377.

45 Y. Jin, L. Dang, H. Zhang, C. Song, Q. Lu and F. Gao, *Chem. Eng. J.*, 2017, **326**, 292–297.

46 R. Gao and D. Yan, *Nano Res.*, 2018, **11**, 1883–1894.

47 S. Su, Q. Zhou, Z. Zeng, D. Hu, X. Wang, M. Jin, X. Gao, R. Notzel, G. Zhou, Z. Zhang and J. Liu, *ACS Appl. Mater. Interfaces*, 2018, **10**, 8026–8035.

48 J. He, X. Liu, H. Liu, Z. Zhao, Y. Ding and J. Luo, *J. Catal.*, 2018, **364**, 125–130.

49 Y. Wang, D. Yan, S. El Hankari, Y. Zou and S. Wang, *Adv. Sci.*, 2018, **5**, 1800064.

50 S. Gao, Z. Sun, W. Liu, X. Jiao, X. Zu, Q. Hu, Y. Sun, T. Yao, W. Zhang, S. Wei and Y. Xie, *Nat. Commun.*, 2017, **8**, 14503.

51 L. Liang, H. Cheng, F. Lei, J. Han, S. Gao, C. Wang, Y. Sun, S. Qamar, S. Wei and Y. Xie, *Angew. Chem., Int. Ed.*, 2015, **54**, 12004–12008.

52 G. Liu, J. Li, J. Fu, G. Jiang, G. Lui, D. Luo, Y. P. Deng, J. Zhang, Z. P. Cano, A. Yu, D. Su, Z. Bai, L. Yang and Z. Chen, *Adv. Mater.*, 2019, **31**, 1806761.

53 Y. Wang, Y. Zhang, Z. Liu, C. Xie, S. Feng, D. Liu, M. Shao and S. Wang, *Angew. Chem., Int. Ed.*, 2017, **56**, 5867–5871.

54 J. Di, J. Xia, M. F. Chisholm, J. Zhong, C. Chen, X. Cao, F. Dong, Z. Chi, H. Chen, Y. X. Weng, J. Xiong, S. Z. Yang, H. Li, Z. Liu and S. Dai, *Adv. Mater.*, 2019, **31**, 1807576.

55 J. Hou, S. Cao, Y. Wu, F. Liang, Y. Sun, Z. Lin and L. Sun, *Nano Energy*, 2017, **32**, 359–366.

56 X. Jiao, Z. Chen, X. Li, Y. Sun, S. Gao, W. Yan, C. Wang, Q. Zhang, Y. Lin, Y. Luo and Y. Xie, *J. Am. Chem. Soc.*, 2017, **139**, 7586–7594.

57 J. Di, C. Chen, S. Z. Yang, S. Chen, M. Duan, J. Xiong, C. Zhu, R. Long, W. Hao, Z. Chi, H. Chen, Y. X. Weng, J. Xia, L. Song, S. Li, H. Li and Z. Liu, *Nat. Commun.*, 2019, **10**, 2840.

58 H. Huang, C. Zhou, X. Jiao, H. Yuan, J. Zhao, C. He, J. Hofkens, M. B. Roeffaers, J. Long and J. A. Steele, *ACS Catal.*, 2020, **10**, 1439–1443.

59 J. Di, C. Chen, C. Zhu, M. Ji, J. Xia, C. Yan, W. Hao, S. Li, H. Li and Z. Liu, *Appl. Catal., B*, 2018, **238**, 119–125.

60 C. K. Chua, Z. Sofer, O. Jankovský and M. Pumera, *ChemPhysChem*, 2015, **16**, 769–774.

61 M. Q. Yang, Y. J. Xu, W. Lu, K. Zeng, H. Zhu, Q. H. Xu and G. W. Ho, *Nat. Commun.*, 2017, **8**, 14224.

62 B. Xu, P. He, H. Liu, P. Wang, G. Zhou and X. Wang, *Angew. Chem., Int. Ed.*, 2014, **53**, 2339–2343.

63 A. Jawaid, D. Nepal, K. Park, M. Jespersen, A. Qualley, P. Mirau, L. F. Drummy and R. A. Vaia, *Chem. Mater.*, 2015, **28**, 337–348.

64 N. K. Oh, H. J. Lee, K. Choi, J. Seo, U. Kim, J. Lee, Y. Choi, S. Jung, J. H. Lee, H. S. Shin and H. Park, *Chem. Mater.*, 2018, **30**, 4658–4666.

65 X. Liu, J. He, S. Zhao, Y. Liu, Z. Zhao, J. Luo, G. Hu, X. Sun and Y. Ding, *Nat. Commun.*, 2018, **9**, 4365.

66 L. Zhang, L. Han, H. Liu, X. Liu and J. Luo, *Angew. Chem., Int. Ed.*, 2017, **56**, 13694–13698.

67 H. Liu, X. Peng, X. Liu, G. Qi and J. Luo, *ChemSusChem*, 2019, **12**, 1334–1341.

68 Y. Liu, C. Liang, J. Wu, T. Sharifi, H. Xu, Y. Nakanishi, Y. Yang, C. F. Woellne, A. Aliyan, A. A. Martí, B. Xie, R. Vajtai, W. Yang and P. M. Ajayan, *Adv. Mater. Interfaces*, 2018, **5**, 1700895.

69 W. Xu, S. Li, S. Zhou, J. K. Lee, S. Wang, S. G. Sarwat, X. Wang, H. Bhaskaran, M. Pasta and J. H. Warner, *ACS Appl. Mater. Interfaces*, 2018, **10**, 4630–4639.

70 C. Zhang, H. Liu, J. He, G. Hu, H. Bao, F. Lü, L. Zhuo, J. Ren, X. Liu and J. Luo, *Electrochem. Commun.*, 2019, **55**, 10511–10514.

71 D. Wang, H. Li, N. Du, Z. Lang, T. Hu and W. Hou, *Adv. Colloid Interface Sci.*, 2019, **541**, 183–191.

72 Q. Zhou, Z. Shen, C. Zhu, J. Li, Z. Ding, P. Wang, F. Pan, Z. Zhang, H. Ma, S. Wang and H. Zhang, *Adv. Mater.*, 2018, **30**, 1800140.

73 K. Jiao, Z. Kang, B. Wang, S. Jiao, Y. Jiang and Z. Hu, *Electroanalysis*, 2018, **30**, 525–532.

74 X. He, S. Z. Luan, L. Wang, R. Y. Wang, P. Du, Y. Y. Xu, H. J. Yang, Y. G. Wang, K. Huang and M. Lei, *Mater. Lett.*, 2019, **244**, 78–82.

75 W. Xu, F. Lyu, Y. Bai, A. Gao, J. Feng, Z. Cai and Y. Yin, *Nano Energy*, 2018, **43**, 110–116.

76 Y. Huo, X. Peng, X. Liu, H. Li and J. Luo, *ACS Appl. Mater. Interfaces*, 2018, **10**, 12618–12625.

77 S. Shen, J. He, X. Peng, W. Xi, L. Zhang, D. Xi, L. Wang, X. Liu and J. Luo, *J. Mater. Chem. A*, 2018, **6**, 18960–18966.

78 F. Lü, G. Qi, X. Liu, C. Zhang, R. Guo, X. Peng, J. He and J. Luo, *Electrochem. Commun.*, 2019, **103**, 127–132.

79 X. Peng, Y. Chen, Y. Mi, L. Zhuo, G. Qi, J. Ren, Y. Qiu, X. Liu and J. Luo, *Inorg. Chem.*, 2019, **58**, 8910–8914.

80 L. Wang, Y. Wang, M. Wu, Z. Wei, C. Cui, M. Mao, J. Zhang, X. Han, Q. Liu and J. Ma, *Small*, 2018, **14**, 1800737.

81 W. Wan, X. Liu, H. Li, X. Peng, D. Xi and J. Luo, *Appl. Catal., B*, 2019, **240**, 193–200.

82 T. Wang, J. Wu, Y. Liu, X. Cui, P. Ding, J. Deng, C. Zha, E. Coy and Y. Li, *Energy Storage Materials*, 2019, **16**, 24–30.

83 K. Uosaki, G. Elumalai, H. Noguchi, T. Masuda, A. Lyalin, A. Nakayama and T. Taketsugu, *J. Am. Chem. Soc.*, 2014, **136**, 6542–6545.

84 Y. Li, C. Zhong, J. Liu, X. Zeng, S. Qu, X. Han, Y. Deng, W. Hu and J. Lu, *Adv. Mater.*, 2018, **30**, 1703657.